Chemical Engineering & Processing: Process Intensification 182 (2022) 109198

Contents lists available at ScienceDirect

Chemical Engineering and Processing - Process Intensification

journal homepage: www.elsevier.com/locate/cep

Microwave-assisted flow synthesis of multicore iron oxide nanoparticles

L. Panariello [a], M.O. Besenhard [a], S. Damilos [a], A. Sergides [b], V. Sebastian [c,d,e,f], S. Irusta [c,d,e,f], J. Tang [a], Nguyen Thi Kim Thanh [b,g], A. Gavriilidis [a,*]

[a] Department of Chemical Engineering, University College London, Torrington Place, London WC1E 7JE, UK
[b] Biophysics Group, Department of Physics and Astronomy, University College London, Gower Street, London WC1E 6BT, UK
[c] Instituto de Nanociencia y Materiales de Aragón (INMA), CSIC-Universidad de Zaragoza, Zaragoza 50009, Spain
[d] Department of Chemical Engineering, University of Zaragoza, Campus Río Ebro-Edificio I+D, C/ Poeta Mariano Esquillor S/N, Zaragoza 50018, Spain
[e] Networking Research Center on Bioengineering, Biomaterials and Nanomedicine, CIBERBBN, Madrid 28029, Spain
[f] Laboratorio de Microscopías Avanzadas, Universidad de Zaragoza, Zaragoza 50018, Spain
[g] UCL Healthcare Biomagnetics and Nanomaterials Laboratories, 21 Albemarle Street, London W1S 4BS, UK

ARTICLE INFO

Keywords:
Magnetic nanomaterials
Flow chemistry
Microwave heating

ABSTRACT

Coprecipitation is by far the most common synthesis method for iron oxide nanoparticles (IONPs). However, reproducibility and scalability represent a major challenge. Therefore, innovative processes for scalable production of IONPs are highly sought after. Here, we explored the combination of microwave heating with a flow reactor producing IONPs through coprecipitation. The synthesis was initially studied in a well-characterised microwave-heated flow system, enabling the synthesis of multicore IONPs, with control over both the single core size and the multicore hydrodynamic diameter. The effect of residence time and microwave power was investigated, enabling the synthesis of multicore nanostructures with hydrodynamic diameter between ~35 and 70 nm, with single core size of 3–5 nm. Compared to particles produced under conventional heating, similar single core sizes were observed, though with smaller hydrodynamic diameters. The process comprised of the initial IONP coprecipitation followed by the addition of the stabiliser (citric acid and dextran). The ability of precisely controlling the stabiliser addition time (distinctive of flow reactors), contributed to the synthesis reproducibility. Finally, scale-up by increasing the reactor length and using a different microwave cavity was demonstrated, producing particles of similar structure as those from the small scale system, with a throughput of 3.3 g/h.

1. Introduction

The use of microwave heating in chemistry is a topic of intense research, particularly in the field of organic chemistry [1] and nanomaterials synthesis [2]. To date, most publications focus on the use of microwave heating in batch systems. The advantage of microwave heating compared to conventional heating (i.e., using heating elements and/or jackets) is the uniform heating of the bulk solution. This reduces temperature inhomogeneities in the solution and yields uniform synthetic conditions, allowing for more controllable and reproducible syntheses. Furthermore, microwave heating can selectively heat a dispersed phase (e.g., catalysts, nanoparticles), and enable faster heating rates than conventional heating (provided a suitable solvent is chosen), which can affect the synthesis kinetics, for instance through faster nucleation rates in colloidal syntheses.

Recently, microwave heating started to be coupled with flow systems, in an attempt to achieve synergistic improvements due to rapid heating rates associated with both technologies. Flow reactors seem to draw benefit from microwave technologies due to the volumetric nature of this type of heating form, with particular benefits towards reactor scale-up [3]. The nature of conventional heating leads to a lower temperature at the centre of a reactor cross section, with the temperature gradient between the outer wall and the centre of the reactor increasing as the reactor radial dimension increases. For a laminar flow reactor, the effect of these gradients on the reactor performance are exacerbated by the higher flow velocity (and hence, volumetric flow rate) at the centre of the reactor. While for microreactors, characterised by high surface-to-volume ratio, the use of conventional heating systems provides high heating rates and uniform (radial) temperature profiles [4], with the increase in the characteristic dimension of the reactor from

* Corresponding author.
E-mail address: a.gavriilidis@ucl.ac.uk (A. Gavriilidis).

https://doi.org/10.1016/j.cep.2022.109198
Received 14 July 2022; Received in revised form 3 October 2022; Accepted 26 October 2022
Available online 30 October 2022

micro- to millifluidic (with capillary diameters ≥ 1 mm) radial temperature uniformity becomes more and more affected. Therefore, millifluidic reactors benefit from microwave heating which has been shown to facilitate faster heating and more uniform radial temperature profiles, as the penetration depth of microwaves in solvents as water is in the order of few centimetres [5]. Focusing on nanomaterials flow synthesis, the bulk heating mechanism of microwave radiation appears to provide another advantage, that is, the reduction of nanoparticle wall deposition, [5,6] one of the major drawbacks of flow technologies in the field of nanomaterials production. Achieving robust water-based synthesis of IONPs can benefit from the use of flow technologies, due to the tight control over process conditions allowed by such micro and millifluidic reactors. Therefore, various IONP syntheses covering water based coprecipitation and partial oxidation, as well as thermal decomposition syntheses in high boiling point solvents have been translated to flow [7–14].

Water-based IONP syntheses often lead to the formation of multicore particle assemblies [15]. These structures are assemblies of smaller particles (i.e., single cores), with varying degree of packing, and are often stabilised by hydrophilic molecules. These include polymers like heparin and carbohydrates like dextran, which adopt different energetically favourable conformations (e.g., coil, brush, mushroom, etc. [16,17]) when dissolved in water, contributing to the formation of cluster-like structures. The clustered nanostructures have interesting properties, for instance in magnetic hyperthermia [18–22] and as MRI contrast agents [23–25]. Reproducible synthesis of multicore structures is a complex task, particularly regarding control over the number of particles composing the assembly [15]. Microwave heating has been successfully applied for this purpose, leading to reproducible synthesis of multicore IONPs via water based batch syntheses [18,26,27].

This work reports the synthesis of multicore IONPs in a microwave-heated flow millireactor. The synthesis was initially performed in a small scale microwave reactor previously developed [28]. We demonstrate the potential of combining microwave heating and flow reactors for IONP coprecipitation, which allowed us to control both the single and multicore nanoparticle sizes. Using a custom-made microwave heating system the small scale IONP synthesis (0.75 mL reactor volume) was scaled up by a factor of 8. The scalability of the microwave flow system developed makes such platform appealing from a production perspective.

2. Materials and methods

2.1. Materials

Ferric chloride hexahydrate ($FeCl_3 \bullet 6H_2O$, ≥97%) was obtained from Alfa Aesar. Ferrous chloride tetrahydrate ($FeCl_2 \bullet 4H_2O$, ≥99%) and sodium hydroxide (NaOH (aq.) standard solution, 2 M) were obtained by Honeywell Fluka. Citric acid monohydrate ($HOC(COOH)(CH_2COOH)_2 \bullet H_2O$, ≥99%) and dextran (from *Leuconostoc* spp., $(C_6H_{10}O_5)_n$, $Mr \sim 6000 M_r \sim 6000$) were obtained from Sigma Aldrich. All chemicals were used as received.

2.2. Particle characterisation

The iron oxide colloidal solution obtained from the flow reactor was collected in glass vials, and was washed twice with acetone (2:1 v:v acetone: colloidal solution) followed by magnetic decantation. High Resolution Transmission Electron Microscopy (HRTEM) was performed using a FEI TITAN^3 operated at 300 kV acceleration voltage. Samples were prepared by dropping the aqueous suspension onto a carbon-coated copper grid (200 mesh) and air dried. Particle size distributions were obtained from the HRTEM images analysing at least 100 particles. The hydrodynamic diameter of the IONPs was measured via dynamic light scattering (DLS) using a DelsaMax Pro (BeckMan Coulter). The colloidal solution was diluted several times until three sequential dilutions gave the same hydrodynamic diameter. The crystal structure and crystallite size of the IONPs were investigated by means of X-ray diffraction (XRD), using a X'Pert diffractometer (Pro-PanAlytical), with Co Kα radiation ($\lambda = 1.79$ Å, 40 kV). XRD patterns were collected from $2\theta = 20^\circ$ to 100° X'Pert High Score plus software equipped with ICSD database was used to identify the XRD patterns. Scherrer's equation was used to calculate the crystallite size of the sample from the XRD pattern, using a peak fitting routine in the commercial software Origin. Fourier transform infrared spectroscopy (FTIR) measurements were performed with a Vertex 70 (Bruker) FTIR spectrometer using an ATR Golden Gate accessory.

2.3. Small scale microwave reactor for IONP synthesis

The small scale microwave flow reactor for IONP coprecipitation used was adapted from previous work [28] and consisted of a 2.4 mm internal diameter (I.D.) PTFE capillary (outer diameter O.D. = 3.2 mm, Thames Restek) placed in a flat PTFE support structure (see Fig. 1). The overall reactor volume under microwave (MW) irradiation V was 0.75 mL (16.5 cm length). The support structure with the capillary was inserted in a commercial single-mode microwave applicator CEM Discover® SP and was placed parallel to the input port of the MW applicator (see Fig. 1). The support structure allowed the reactive stream to enter and exit the cavity from the top of the MW cavity.

The IONPs were synthesised following the coprecipitation protocol described by Besenhard *et al.* [29] with the addition of dextran to the stabilisation solution. In a standard synthesis, two glass syringes (Scientific Glass Engineering) were filled respectively with a 0.1 M aqueous iron chlorides solution ($FeCl_3$:$FeCl_2$=2:1 mol:mol) and a 0.57 M sodium hydroxide solution. The two solutions were delivered by a syringe pump (KD Scientific Legato 270P) to an ETFE T-mixer (0.5 mm I.D., Upchurch) connected to the inlet of the microwave-heated reactor through a 10 cm PTFE capillary (0.5 mm I.D.). The flow rate in the microwave-heated system was varied between 10, 5, and 2.5 mL/min (total flow rate is the sum of the flow rates of iron precursor and base), corresponding to an average residence time in the microwave-heated reactor of 4.5, 9 and 18 s. The microwave power input was tuned between 0, 5 and 10 W for each flow rate (except for a flow rate of 2.5 mL/min, where the maximum power output was set as 5 W). These power settings led to different outlet temperatures, between room temperature and 60 °C, comparable to those employed by Besenhard *et al.* A second identical T-mixer was connected to the outlet of the microwave-heated capillary (2.4 mm I.D., Thames Restek), at 5 cm from the end of the microwave-irradiated zone). The colloidal iron oxide solution exiting the reactor was mixed with an aqueous solution containing dextran (6 mM) and citric acid (0.29 M) to stabilise the IONPs. The stabiliser solution was delivered to the second T-mixer from a third glass syringe (Scientific Glass Engineering) secured to a second syringe pump (Harvard Apparatus PHD 2000). The stabiliser was added after particle precipitation (rather than added to the iron precursor feed) following the protocol from Besenhard *et al.* [29], who demonstrated that greater colloidal stability is achieved by precipitating the IONPs at high pH and subsequently lowering the pH via the addition of an acidic stabiliser. The ratio between the volumetric flowrate of the IONP solution and that of the dextran/citric acid solution was kept equal to 5:1 (v:v) for all the IONP syntheses performed. A schematic of the flow system is provided in Fig. 1. This system was modified following the approach of Bayazit *et al.* [30] to allow temperature measurement of the product stream at the microwave cavity outlet. A T-connector was connected to the outlet of the capillary reactor (before the stabiliser stream mixes with the colloidal solution) hosting a thermocouple (K Type), allowing the measurement of the product stream temperature prior to the injection of the stabiliser solution. For every experiment, the system was operated for three times the average residence time to allow for steady state operation to be reached, then 20 mL samples were collected. Reproducibility was analysed performing three independent experiments in

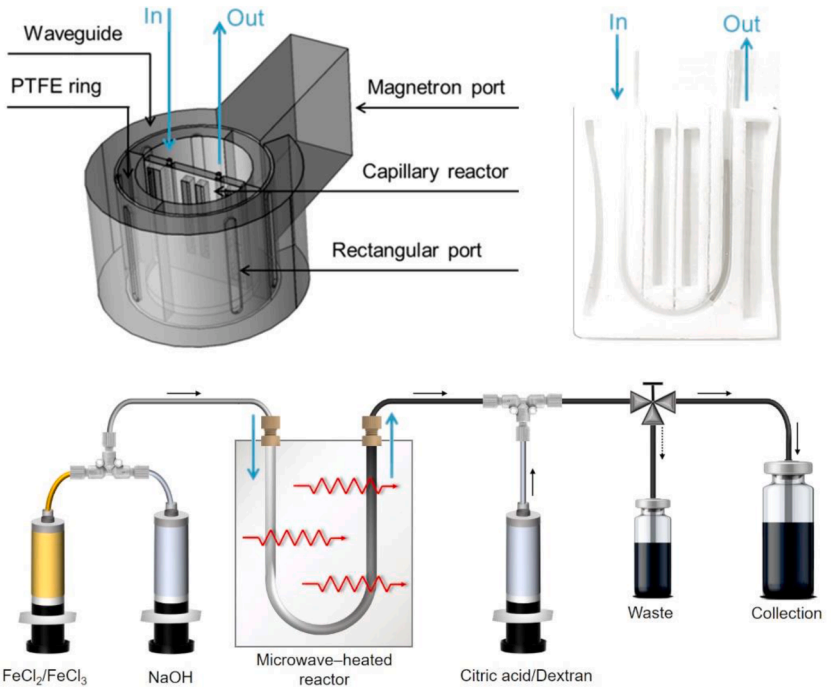

Fig. 1. Top: Schematic of the small scale microwave-heated flow reactor. Bottom: Schematic of the set-up used for the synthesis of iron oxide nanoparticles.

different days and characterising samples via DLS after magnetically washing the colloid (see Section 2.2).

2.4. Scaled-up microwave reactor for IONP synthesis

The IONP synthesis was scaled-up by increasing the reactor volume under MW irradiation from 0.75 mL to 6 mL, achieved by increasing the length of the reactor to 1.32 m, while keeping the tube diameter constant (2.4 mm I.D.). The reactor configuration was changed from a U-shaped capillary (used in the small scale microwave reactor) to a helical coil. The coil was supported on a PTFE rod (2.5 cm diameter) and was enclosed in expanded polystyrene (EPS) to improve thermal insulation. The reactor was placed in a single mode microwave cavity (Sairem, Spin Reactor) powered by a solid-state conductor generator (Sairem, GMS450) operating between 2.4 and 2.5 GHz, with a maximum power output of 450 W. The microwave cavity hosting the reactor was a TE10 monomode cavity with a W340 waveguide. The power reflected to the generator could be minimised thanks to three stab-tuners placed between the generator and the reactor and a sliding short circuit closing the cavity. The front of the reactor could be directly observed thanks to a circular window in the cavity, allowing the measurement of the reactor temperature via an infrared (IR) camera (Optris PI400). A port of ~ 0.5 cm was made in the EPS insulation to allow for temperature measurement via IR imaging. The use of a rectangular waveguide with access ports both on the top and bottom of the cavity (see Fig. 2) facilitated the use of the coiled reactor configuration of larger overall volume. Furthermore, the ability of reducing the power reflected to the microwave generator enabled prolonged operation as a result of the minimal

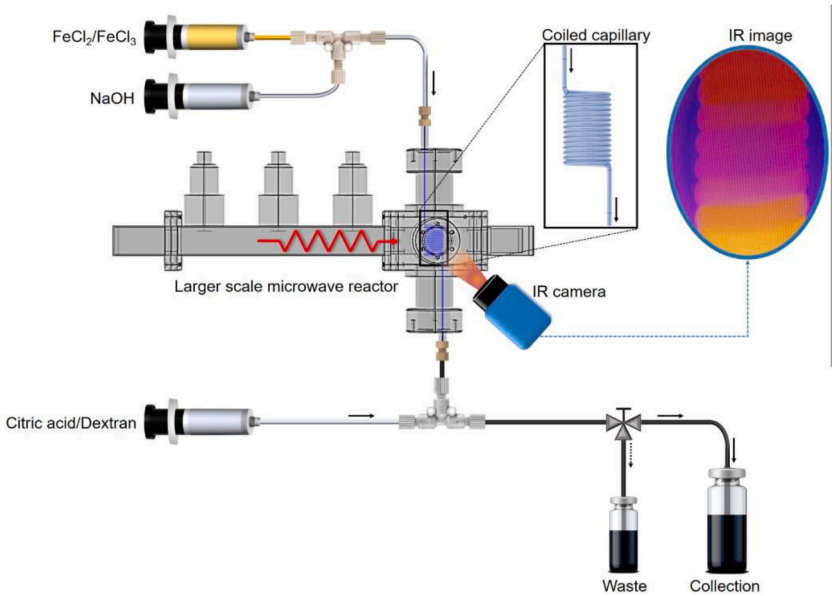

Fig. 2. Schematic of the scaled-up system for the microwave-assisted continuous synthesis of iron oxide nanoparticles.

increase in the temperature of the generator. This feature also resulted in a more robust power output, as increase in the generator temperature causes fluctuations in the generator output. A schematic of the experimental set-up is shown in Fig. 2. The inlet of the reactor coil (the capillary inserted in the larger scale microwave reactor) was connected to a PEEK T-mixer (1 mm I.D., Upchurch), in which the iron precursor and base solutions were mixed. These two solutions (same concentration as in Section 2.3) were delivered to the T-mixer by means of a syringe pump (Harvard PhD Ultra), which housed two glass syringes (100 mL Scientific Glass Engineering) filled with the two solutions (iron precursor and base). The total flow rate (sum of the iron precursor and base streams) was set to 20 mL/min, leading to an average residence time in the coiled reactor of 18 s. The mixing time at the flow rates used was estimated to be 40 ms based on the correlation provided by Falk and Commenge [31]. The T-mixer was connected to the MW irradiated region by means of a 10 cm long, 1 mm I.D. capillary. The microwave system was operated with a 50 W power input, leading to an outlet temperature of 53 °C. The outlet of the reactor coil was connected to a second PEEK T-mixer (1 mm I.D., Upchurch) where the colloidal solution coming out of the reactor was mixed with the stabilisation solution (citric acid and dextran) at the same concentration and flow ratio between colloidal solution and stabiliser streams used for the small scale system. The stabiliser solution was delivered to the junction using a second syringe pump (Harvard PhD Ultra) housing a 50 mL glass syringe (Scientific Glass Engineering) filled with the stabiliser solution. As the small scale reactor, the system was operated for three average residence times and then 20 mL samples were collected for characterisation. Three independent experiments were performed, and samples were analysed via DLS to confirm reproducibility, after magnetically washing the samples (see Section 2.2).

3. Results and discussion

3.1. IONP synthesis in the small scale microwave reactor

One of the main issues for the implementation of iron oxide coprecipitation reactions in capillary flow reactors is channel blockage, due to the precipitation of micron-sized aggregates of IONPs upon mixing the reagents and before stabilisation. Following the approach proposed by Uson *et al.* [14], we identified the minimum flow rate (in this case equal to 2.5 mL/min) providing enough inertia to the fluid to push the precipitating aggregates (and possible sediments) through the channel without clogging. Below this flow rate stable operation of the reactor could not be achieved. This flowrate defines the maximum residence time τ at which the system can be operated, equal to 18 s. This was calculated as the ratio between the reactor volume V and the total flow rate Q. The three flow rates tested, namely 10, 5 and 2.5 mL/min, gave residence times in the microwave heated region of $\tau = 4.5$, 9 and 18 s, corresponding to mixing times between 20 ms and 68 ms [31]. To achieve an outlet temperature between room temperature and 60 °C, i.e., what was previously used with conventional heating [29], the power applied was varied between 0 and 10 W. The exception was the 18 s synthesis, where 5 W already led to an outlet temperature of $\sim 60^{\circ}C \sim$ 60 °C. With this combination of applied powers and residence times, the synthesis was performed at various outlet temperatures, ranging between room temperature and 60 °C. In all the 8 synthetic conditions tested, XRD revealed the formation of magnetite/maghemite nanoparticles (see Supporting Information S1). Table 1 summarises the results of the experiments in terms of size of the nanostructures. The significantly higher value of the hydrodynamic diameter D_H compared to the TEM size d_{TEM} suggests that the particles are assembled as multicore structures. This is not surprising, as dextran, utilised to stabilise the particles, has been reported to generate multicore assemblies of IONPs [26]. The values of D_H were highly reproducible, with relative standard deviation after three independent runs in the order of 5%.

These IONP aggregates can be described through fractal geometry, with the size of the aggregate D_H depending on the number N and size d_{TEM} of the single particles composing the aggregate, according to [32]:

$$N = K\left(\frac{D_H}{d_{TEM}}\right)^{d_f} \quad (1)$$

where K is the fractal prefactor and d_f is the fractal dimension of the colloidal aggregate. Here K was assumed equal to 1 (generally this value ranges between 1 and 1.2) and $d_f = 3$ (spherical packing) [32]. Using (1) one can estimate the number of cores composing the multicore assembly.

Table 1
Hydrodynamic diameter D_H (multicore), crystallite size d_{XRD}, TEM-derived particle size d_{TEM} (single core) and number of cores composing the multicore structure N for the experiments performed. The error with respect to D_H represents the standard deviation after three independent repeats of the syntheses.

Power [W]	Residence time τ [s]	Outlet temperature [°C]	D_H [nm]	d_{XRD} [nm]	d_{TEM} [nm]	N [-]
0	4.5	25	31.4 ± 0.7	3.2	3.1	909
5	4.5	29.8	34.6 ± 0.5	3.1	3.2	1319
10	4.5	40.9	40.3 ± 0.5	4.1	4.6	928
0	9	25	34.5 ± 0.8	3.1	3.8	1319
5	9	34.4	49.3 ± 0.3	4.1	4.1	1504
10	9	53.9	55.1 ± 0.5	4.8	4.7	1504
0	18	25	48.7 ± 0.7	4	4	1728
5	18	56.5	70.5 ± 1	5.3	5.6	2404

Fig. 3(a), (b) show that both D_H and d_{TEM} increase with the increase of both power and residence time. The residence time has a positive effect on the size of the nanostructure, as one can see for the 0 W condition (i.e., room temperature synthesis), where an increase in both D_H and d_{TEM} is observed for increasing τ. For a given residence time, the increase in power translates in an increase in temperature (Fig. 3(c)), which results in a corresponding increase in both hydrodynamic and single core sizes. These results are consistent with the literature. The IONP formation mechanism in coprecipitation syntheses is an aggregative process involving intermediate iron oxide and hydroxide phases [29,33–35]. For a rapid base addition, as studied here, magnetite/maghemite is not forming directly when the iron precursor and base solutions are mixed, but forms from the initially precipitated crystalline and/or amorphous intermediate phases (depending on the synthetic conditions). For the system studied magnetite/maghemite formation is expected to occur within 3 s (at 60 °C) and within ~30 s at room temperature [36]. Hence higher temperature (as well as higher pH) results in faster magnetite/maghemite formation [37,38]. The temperature dependant particle formation kinetics with timescales comparable to the residence time, involving intermediate phases which are likely to have different aggregation likelihoods, explains the sensitivity of IONP properties (e.g., single and multicore dimensions) to the synthetic conditions. For example, the smaller single core dimensions at lower temperatures can be related to incomplete transition of intermediate phases to magnetite/maghemite and their dissolution after the addition of citric acid, as previously discussed [36]. Even though a definitive model describing the relation between nucleation-aggregation-growth kinetics and particle size distribution for the system studied has not been reported, results from the literature indicate that an increase in temperature leads to an increase in the particle size [39], consistently with an aggregative mechanism, where the aggregation rate increases as a function of the temperature [37,40–42]. The ability of sequentially

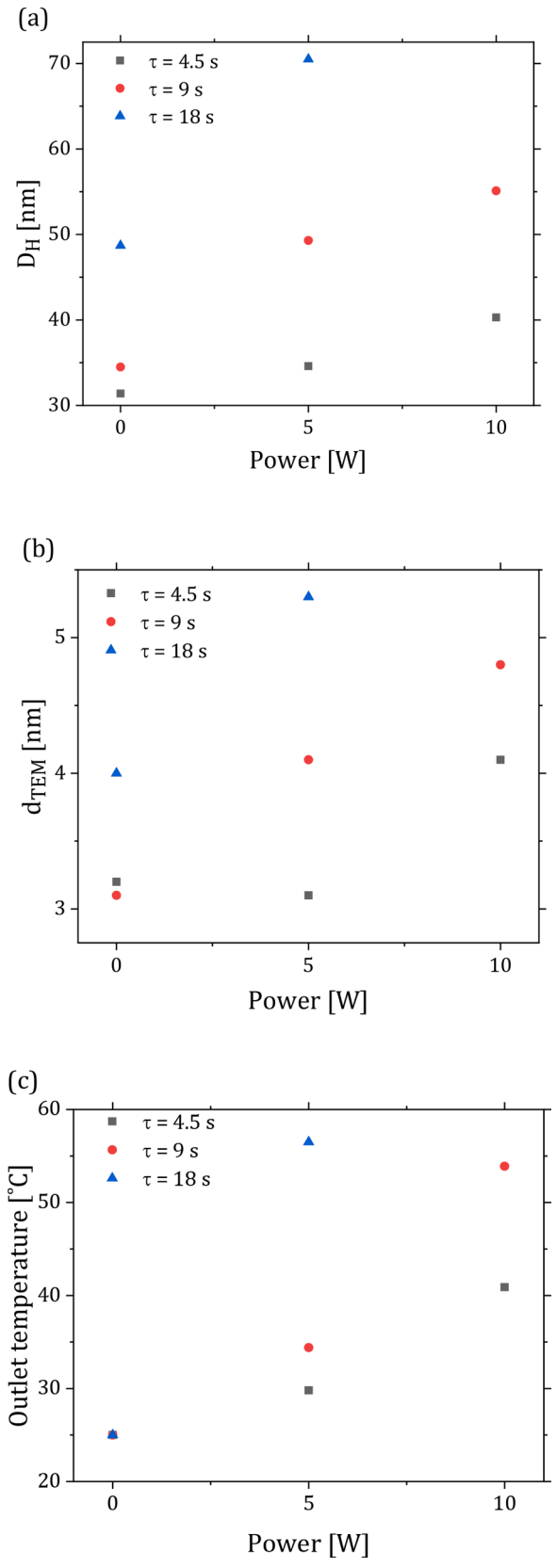

Fig. 3. (a) Hydrodynamic diameter D_H, (b) TEM size d_{TEM} and (c) reactor outlet temperature as a function of the applied power for the different residence times tested.

adding citric acid to the solution offered by flow reactors allows for precise quenching of the reaction, as citric acid can both coat the IONPs and chelate the iron ions in solution preventing them to react any further [43]. This enables us to control the size down to values hardly achievable in batch under similar conditions [43]. On the other hand, the use of dextran promotes the formation and stabilisation of the multicore structures, as hydrophilic polymers like dextran act as a backbone to cluster the iron oxide particles and support the architecture in water [15, 23].

Similar experiments performed by Besenhard *et al.* [29,36] under conventional heating led to particles with similar sizes, with $d_{TEM} = 5$ to 8 nm depending on the time interval between the initial particle precipitation (mixing the precursor and base solution) and stabilisation (adding the stabilisation solution), with the smallest core size observed for the shortest time interval of 5 s. However, significantly smaller D_H was observed under conventional heating, in the order of $20 - 40$ nm (see Table 2). A wider range of multicore diameters was achieved in the microwave reactor, yielding D_H values between from 30 to 70 nm. We hypothesise that the higher hydrodynamic diameter could be related to the different heating rates and possible effects of alternating electric field on colloid dynamics [44], resulting in different particle formation kinetics, and a different interplay between aggregation and growth of the intermediate phases involved and already formed magnetite/maghemite. In particular, the microwave- and conventionally-heated systems compared here are characterised by different temperature profiles, where the U-shaped microwave reactor exhibits a sigmoidal temperature profile along the reactor axis [28], while the conventional system is characterised by an isothermal profile. This difference results in different conditions at which the particles nucleate and grow. In Besenhard *et al.* [29] the precursor and base were preheated and then mixed, hence the IONPs would nucleate and grow at the reaction temperature, whereas in the experiments reported here the particles nucleate at room temperature (as suggested by the immediate appearance of a black solution right after the mixing junction at room temperature), and the solution is subsequently heated by microwave radiation. This approach is particularly suited for microwave heating technologies, where a faster heating rate can be achieved when compared to conventional heating systems [5].

The nanoparticle crystallite sizes d_{XRD} closely match those obtained from HRTEM images, d_{TEM} (see Table 1, Fig. 4 and Supporting Information S2). The particles appear as single crystals, as one can observe from Fig. 4, supporting the similarity between the XRD and TEM diameters. The lattice spacing measured in Fig. 4(c) and (f) (0.29 nm and 0.25 nm respectively) matches the (2 2 0) and (3 1 1) planes characteristic of magnetite/maghemite [45], in agreement with the XRD pattern, where only magnetite/maghemite peaks were detected (Supporting Information S1).

The presence of both dextran and citric acid on the surface of the assemblies was confirmed via ATR-FTIR spectroscopy (Figs. 5 and Supporting Information S3). In order to remove artifacts induced by the presence of adsorbed water molecules, the samples were freeze-dried before characterisation.

Table 2
Comparison between flow produced iron oxide nanoparticles obtained via aqueous coprecipitation reactions with similar protocols using the conventionally heated reactor described in Besenhard *et al.* [29,36], the small scale microwave reactor system, and the scaled-up microwave reactor system in this work.

	Besenhard *et al.* [36].	Besenhard *et al.* [29].	Small scale microwave system	Scaled-up microwave system
τ [s]	5	100	18	18
Outlet temperature [°C]	60	60	56.5	53
D_H [nm]	19	19.1	70.5	60
d_{XRD} [nm]	5.1	6.9	5.3	5.9

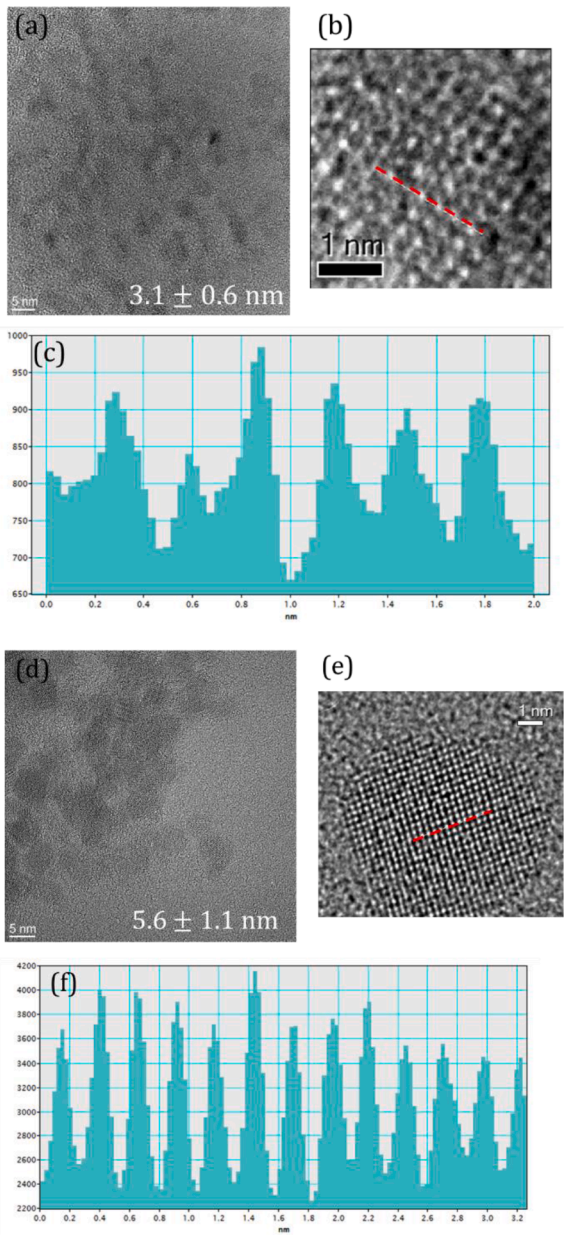

Fig. 4. (a) HRTEM image of iron oxide nanoparticles produced with $\tau = 4.5$ s and power = 0 W and (b) single nanoparticle image with (c) corresponding lattice spacing profile. (d) HRTEM image of iron oxide nanoparticles produced with $\tau = 18$ s and power = 5 W and (e) single nanoparticle image with (f) corresponding lattice spacing profile. Lattice spacing profiles refer to the red-line shown on the single nanoparticle images and were obtained from the greyscale intensity along these lines.

The main characteristic bands for dextran, observed at 1147, 1105 and 1012 cm^{-1}, can be assigned respectively to stretching vibrations of the C − O − C bond and glycosidic bridge, stretching vibration of the C −O bond at the C4 position of glucose residue and the great chain flexibility present in dextran around α (1 → 6) glycoside bonds [46]. Peaks at 1420 and 1344 cm^{-1} are related to ν(C −H) vibrational modes [47]. The broad band centred around 3370 cm^{-1} can be assigned to the hydroxyl stretching vibration of the polysaccharide, with possible contribution from absorbed water [47]. The C − H and carboxyl group stretching vibrations appear in regions 3000–2800 and 1790–1590 cm^{-1} respectively (Fig. 5(b)). The citric acid spectrum shows peaks at 1752, 1722 and 1690 cm^{-1} due to stretching vibrations of the C = O bond of COOH groups. The peak at 1211 cm^{-1} can be assigned to symmetric

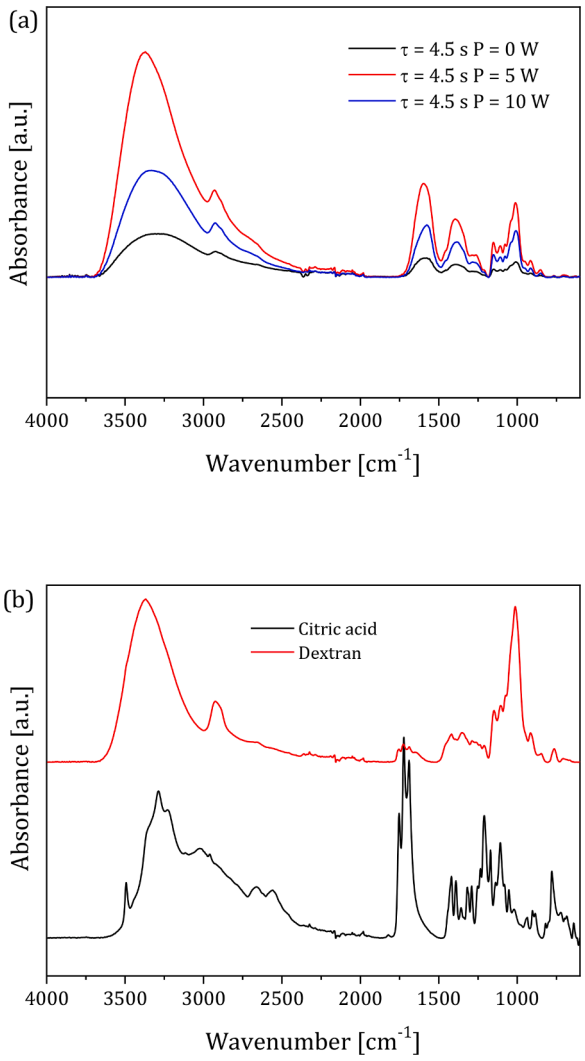

Fig. 5. ATR-FTIR spectra of (a) iron oxide nanoparticles ($\tau = 4.5$ s, power = 0 − 10 W) and (b) dextran and citric acid powders.

stretching of C − O, the peaks that appear at 3020 cm^{-1} and 2960 cm^{-1} are due to CH_2 groups of citric acid, while the peaks at 3493 and 3287 cm^{-1} are due to OH groups vibrations (Fig. 5(b)) [48]. FTIR spectra of (washed and dried) IONP samples (Fig. 5(a) and Supporting Information S3) show a broad band in the range 3670–3000 cm^{-1} that could be assigned to O − H stretching vibrations that would be related to the presence of dextran, but the contribution of adsorbed water cannot be ruled out. The dextran bands in the range 3000–2800 cm^{-1} related to C − H stretching vibration confirm the presence of the organic compound, as well as the characteristic bands at 1147, 1105 and 1012 cm^{-1}. A new broad band with maximum around 1600 cm^{-1} can be observed in all the sample spectra. The assignment of this signal is not clear, and it could be related to O − H bending vibration from absorbed water.

3.2. IONP synthesis in the scaled-up microwave reactor

Microwave heating holds great promise for the efficient scale-up of flow systems, due to its volumetric nature and fast temperature ramping. Therefore, the scale-up of the microwave-heated reactor was investigated. The synthesis performed in the small scale microwave reactor at $\tau = 18$ s and 5 W was scaled-up using a second microwave-heated reactor (described above), increasing the flow rate from 2.5 mL/min (150 mL/h) to 20 mL/min (1.2 L/h). This increase translates in a theoretical increase in Fe mass throughput from ~0.4 g/h to ~3.3 g/h.

The residence time was kept constant between the two systems by increasing the volume of the reactor. The temperature at the reactor outlet was maintained similar to that of the small scale system ($\sim 56^{\circ}C \sim 56$ °C) by increasing the power applied. The reactor surface temperature was measured with an IR camera (see Fig. 6(a)), indicating that a temperature of 53 °C was achieved at the reactor outlet by applying 50 W and properly tuning the position of the sliding short circuit and stab tuners in order to reduce the power reflected to the generator to 1 W (as measured by the generator).

The particles were characterised via XRD, showing that the crystal structure matched that of magnetite/maghemite (Fig. 6(b)). The crystallite size and the hydrodynamic diameter of the particles produced in the scaled-up reactor system were respectively equal to $d_{XRD} = 5.9$ nm and $D_H = 60$ nm, against $d_{XRD} = 5.3$ nm and $D_H = 70$ nm obtained using the small scale system (see Table 2), i.e., a difference of $\sim 14\%$. The small deviation may be related to non-negligible secondary flows due to the geometrical configuration of the coiled tube [5,49], which are expected to alter the transport phenomena within the reactor, as well as differences in the heating profiles between the two set-ups.

4. Conclusions

This work presents the synthesis of iron oxide nanoparticles via an aqueous coprecipitation reaction in a microwave-heated flow reactor. Different reactor residence times and applied microwave powers were tested. The reactor was operated without channel blockage by properly tuning the flow rate to achieve sufficiently high shear to prevent particle deposition at the tube wall. The synthesis performed in the microwave-heated system led to the formation of multicore structures composed of several single core iron oxide nanoparticles. The hydrodynamic diameter of the structures was tuned between 30 and 70 nm by changing the residence time and the microwave power applied. The precise addition of citric acid and dextran at the reactor outlet allowed to timely quench the process, to enable fine tuning of the single core size between ~ 3 and 5 nm. The scale-up of the microwave-heated reactor was investigated by increasing the reactor length and employing a different microwave cavity to host the larger reactor. Despite the significant changes in the experimental set-up, the product obtained from the scaled-up system showed similar size as the one obtained from the small scale reactor, with only $\sim 14\%$ change in the multicore hydrodynamic diameter and single core size, showing the robustness of the proposed synthetic protocol. When comparing the microwave-assisted synthesis with results from the literature under similar conditions but with conventional heating, a systematic increase in the hydrodynamic diameter was observed, whereas the single core sizes appear similar. This finding suggests a change in the nucleation and/or aggregation rates determining the synthesis outcome, possibly related to different temperature profile within the microwave-heated reactor, as compared to conventionally heated systems.

CRediT authorship contribution statement

L. Panariello: Investigation, Data curation, Conceptualization, Visualization, Writing – original draft. **M.O. Besenhard:** Investigation, Visualization, Writing – review & editing. **S. Damilos:** Investigation. **A. Sergides:** Investigation. **V. Sebastian:** Investigation, Writing – review & editing. **S. Irusta:** Investigation, Writing – review & editing. **J. Tang:** Writing – review & editing, Resources. **Nguyen Thi Kim Thanh:** Writing – review & editing. **A. Gavriilidis:** Conceptualization, Supervision, Resources, Funding acquisition, Writing – review & editing.

Declaration of Competing Interest

The authors declare that they have no known competing financial interests or personal relationships that could have appeared to influence the work reported in this paper.

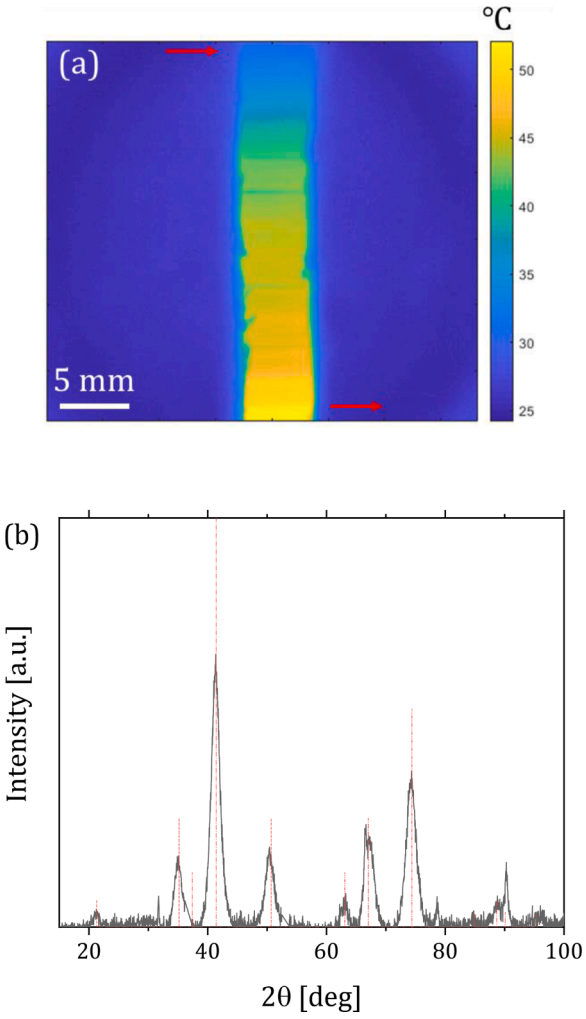

Fig. 6. (a) IR image of the reactor as observed from the frontal port of the custom-made Sairem microwave system. The arrows represent the direction of the flow in the reactor coil. (b) XRD diffractogram of the particles obtained with the red lines representing the reference peaks for magnetite/maghemite (pdf ref. 03–065–3107). Reactor operated with power = 50 W, flow rate = 20 mL/min, outlet temperature = 53 °C, average residence time $\tau = 18$ s.

Data Availability

Data will be made available on request.

Acknowledgments

L.P. received funding from the European Union's Horizon 2020 research and innovation programme under the Marie Skłodowska-Curie Grant Agreement No. 721290. This publication reflects only the authors' view, exempting the Community from any liability. Project website: http://cosmic-etn.eu/. We also thank EPSRC (Grant EP/M015157/1) for funding. AS thanks the EPSRC CDT for the Advanced Characterization of Materials (grant EP/L015277/1) for his studentship. VS acknowledges the ICTS ELECMI-LMA for offering access to their instruments and expertise.

Supplementary materials

Supplementary material associated with this article can be found, in the online version, at doi:10.1016/j.cep.2022.109198.

References

[1] C.O. Kappe, D. Dallinger, The impact of microwave synthesis on drug discovery, Nat. Rev. Drug Discov. 5 (2006) 51–63.

[2] M. Baghbanzadeh, L. Carbone, P.D. Cozzoli, C.O. Kappe, Microwave-assisted synthesis of colloidal inorganic nanocrystals, Angew. Chem. Int. Ed. 50 (2011) 11312–11359.

[3] J.P. Barham, E. Koyama, Y. Norikane, N. Ohneda, T. Yoshimura, Microwave flow: a perspective on reactor and microwave configurations and the emergence of tunable single-mode heating toward large-scale applications, Chem. Rec. 19 (2019) 188–203.

[4] T.N. Glasnov, C.O. Kappe, The microwave-to-flow paradigm: translating high-temperature batch microwave chemistry to scalable continuous-flow processes, Chem. A Eur. J. 17 (2011) 11956–11968.

[5] R. Manno, V. Sebastian, R. Mallada, J. Santamaria, 110th Anniversary: nucleation of Ag nanoparticles in helical microfluidic reactor. Comparison between microwave and conventional heating, Ind. Eng. Chem. Res. 58 (2020) 12702–12711.

[6] S. Horikoshi, T. Sumi, N. Serpone, A hybrid microreactor/microwave high-pressure flow system of a novel concept design and its application to the synthesis of silver nanoparticles, Chem. Eng. Process. Process Intensif. 73 (2013) 59–66.

[7] A. Abou Hassan, O. Sandre, V. Cabuil, P. Tabeling, Synthesis of iron oxide nanoparticles in a microfluidic device: preliminary results in a coaxial flow millichannel, Chem. Commun 15 (2008) 1783–1785.

[8] A. Abou-Hassan, J.F. Dufrêchfer, O. Sandre, G. Mériguet, O. Bernard, V. Cabuil, Fluorescence confocal laser scanning microscopy for pH mapping in a coaxial flow microreactor: application in the synthesis of superparamagnetic nanoparticles, J. Phys. Chem. C 113 (2009) 18097–18105.

[9] L. Frenz, A. El Harrak, M. Pauly, S. Bégin-Colin, A.D. Griffiths, J.C. Baret, Droplet-based microreactors for the synthesis of magnetic iron oxide nanoparticles, Angew. Chem. Int. Ed. 47 (2008) 6817–6820.

[10] K. Kumar, A.M. Nightingale, S.H. Krishnadasan, N. Kamaly, M. Wylenzinska-Arridge, K. Zeissler, W.R. Branford, E. Ware, A.J. DeMello, J.C. DeMello, Direct synthesis of dextran-coated superparamagnetic iron oxide nanoparticles in a capillary-based droplet reactor, J. Mater. Chem. 22 (2012) 4704–4708.

[11] L. Panariello, G. Wu, M.O. Besenhard, K. Loizou, L. Storozhuk, N.T.K. Thanh, A. Gavriilidis, A modular millifluidic platform for the synthesis of iron oxide nanoparticles with control over dissolved gas and flow configuration, Mater 13 (2020) 1019 (Basel, Switzerland)19 pp.

[12] M.O. Besenhard, A.P. Lagrow, S. Famiani, M. Pucciarelli, P. Lettieri, N.T.K. Thanh, A. Gavriilidis, Continuous production of iron oxide nanoparticles via fast and economical high temperature synthesis, React. Chem. Eng. 5 (2020) 1474–1483.

[13] B. Enzo, S. Neveu, A. Abou-Hassan, High temperature continuous flow syntheses of iron oxide nanoflowers using the polyol route in a multi-parametric millifluidic device, Nanomaterials 12 (2022) 119, 18 pp.

[14] L. Uson, M. Arruebo, V. Sebastian, J. Santamaria, Single phase microreactor for the continuous, high-temperature synthesis of <4nm superparamagnetic iron oxide nanoparticles, Chem. Eng. J. 340 (2018) 66–72.

[15] L. Gutiérrez, R. Costo, C. Grüttner, F. Westphal, N. Gehrke, D. Heinke, A. Fornara, Q.A. Pankhurst, C. Johansson, S. Veintemillas-Verdaguer, M.P. Morales, Synthesis methods to prepare single- and multi-core iron oxide nanoparticles for biomedical applications, Dalt. Trans. 44 (2015) 2943–2952.

[16] D. Sarkar, P. Somasundaran, Conformational dynamics of poly (acrylic acid). A study using surface plasmon resonance spectroscopy, Langmuir 20 (2004) 4657–4664.

[17] E.P.K. Currie, W. Norde, M.A.C. Cohen Stuart, Tethered polymer chains: surface chemistry and their impact on colloidal and surface properties, Adv. Colloid Interface Sci. 100 (102) (2003) 205–265.

[18] C. Blanco-Andujar, D. Ortega, P. Southern, Q.A. Pankhurst, N.T.K. Thanh, High performance multi-core iron oxide nanoparticles for magnetic hyperthermia: microwave synthesis, and the role of core-to-core interactions, Nanoscale 7 (2015) 1768–1775.

[19] S. Dutz, M. Kettering, I. Hilger, R. Müller, M. Zeisberger, Magnetic multicore nanoparticles for hyperthermia-influence of particle immobilization in tumour tissue on magnetic properties, Nanotechnology 22 (2011), 265102, 7 pp.

[20] L. Lartigue, P. Hugounenq, D. Alloyeau, S.P. Clarke, M. Lévy, J.C. Bacri, R. Bazzi, D.F. Brougham, C. Wilhelm, F. Gazeau, Cooperative organization in iron oxide multi-core nanoparticles potentiates their efficiency as heating mediators and MRI contrast agents, ACS Nano 6 (2012) 10935–10949.

[21] L. Storozhuk, M.O. Besenhard, S. Mourdikoudis, A.P. Lagrow, M.R. Lees, L.D. Tung, A. Gavriilidis, N.T.K. Thanh, Stable iron oxide nanoflowers with exceptional magnetic heating efficiency: simple and fast polyol synthesis, ACS Appl. Mater. Interfaces 13 (2021) 45870–45880.

[22] H. Gavilan, E.H. Sanchez, M.E.F. Brollo, L. Asin, K.K. Moerner, C. Frandsen, F. J. Lazaro, C.J. Serna, S. Veintemillas-Verdaguer, M.P. Morales, L. Gutierrez, Formation mechanism of maghemite nanoflowers synthesized by a polyol-mediated process, ACS Omega 2 (2017) 7172–7184.

[23] A.M. King, C. Bray, S.C.L. Hall, J.C. Bear, L.K. Bogart, S. Perrier, G.L. Davies, Exploring precision polymers to fine-tune magnetic resonance imaging properties of iron oxide nanoparticles, J. Colloid Interface Sci. 579 (2020) 401–411.

[24] A. Roch, Y. Gossuin, R.N. Muller, P. Gillis, Superparamagnetic colloid suspensions: water magnetic relaxation and clustering, J. Magn. Magn. Mater. 293 (2005) 532–539.

[25] M. Lévy, F. Gazeau, C. Wilhelm, S. Neveu, M. Devaud, P. Levitz, Revisiting MRI contrast properties of nanoparticles: beyond the superparamagnetic regime, J. Phys. Chem. C 117 (2013) 15369–15374.

[26] R.M. Wong, D.A. Gilbert, K. Liu, A.Y. Louie, Rapid size-controlled synthesis of dextran-coated, 64Cu-doped iron oxide nanoparticles, ACS Nano 6 (2012) 3461–3467.

[27] E.A. Osborne, T.M. Atkins, D.A. Gilbert, S.M. Kauzlarich, K. Liu, A.Y. Louie, Rapid microwave-assisted synthesis of dextran-coated iron oxide nanoparticles for magnetic resonance imaging, Nanotechnology 23 (2012), 215602, 9 pp.

[28] S. Damilos, A.N.P. Radhakrishnan, G. Dimitrakis, J. Tang, A. Gavriilidis, Experimental and computational investigation of heat transfer in a microwave-assisted flow system, Chem. Eng. Process. Process Intensif. 142 (2019), 107537, 9 pp.

[29] M.O. Besenhard, A.P. Lagrow, A. Hodzic, M. Kriechbaum, L. Panariello, G. Bais, K. Loizou, S. Damilos, N.T.K. Thanh, A. Gavriilidis, Co-precipitation synthesis of iron oxide nanoparticles with NaOH: new insights and production via flow chemistry, Chem. Eng. J. 399 (2020), 125740, 9 pp.

[30] M.K. Bayazit, J. Yue, E. Cao, A. Gavriilidis, J. Tang, Controllable synthesis of gold nanoparticles in aqueous solution by microwave assisted flow chemistry, ACS Sustain. Chem. Eng 4 (2016) 6435–6442.

[31] L. Falk, J.M. Commenge, Performance comparison of micromixers, Chem. Eng. Sci. 65 (2010) 405–411.

[32] S. Lazzari, L. Nicoud, B. Jaquet, M. Lattuada, M. Morbidelli, Fractal-like structures in colloid science, Adv. Colloid Interface Sci. 235 (2016) 1–13.

[33] J. Baumgartner, A. Dey, P.H.H. Bomans, C.Le Coadou, P. Fratzl, N.A.J. M. Sommerdijk, D. Faivre, Nucleation and growth of magnetite from solution, Nat. Mater. 12 (2013) 310–314.

[34] M. Widdart, E. Schneck, V. Reichel, J. Baumgartner, L. Bertinetti, W. Habraken, K. Bente, P. Fratzl, D. Faivre, Combined experimental and theoretical approach to the kinetics of magnetite crystal growth from primary particles, J. Phys. Chem. Lett. 8 (2017) 1132–1136.

[35] J.P. Jolivet, C. Chanéac, E. Tronc, Iron oxide chemistry. From molecular clusters to extended solid networks, Chem. Commun. (2004) 477–483.

[36] M.O. Besenhard, L. Panariello, C. Kiefer, A.P. Lagrow, L. Storozhuk, F. Perton, S. Begin, D. Mertz, N.T.K. Thanh, A. Gavriilidis, Small iron oxide nanoparticles as MRI T1 contrast agent: scalable inexpensive water-based synthesis using a flow reactor, Nanoscale 13 (2021) 8795.

[37] M.O. Besenhard, D. Jiang, Q.A. Pankhurst, P. Southern, S. Damilos, L. Storozhuk, A. Demosthenous, N.T.K. Thanh, P. Dobson, A. Gavriilidis, Development of an in-line magnetometer for flow chemistry and its demonstration for magnetic nanoparticle synthesis, Lab Chip 21 (2021) 3775–3783.

[38] G. Gkogkos, M.O. Besenhard, L. Storozhuk, N.T.K. Thanh, A. Gavriilidis, Fouling-proof triple stream 3D flow focusing based reactor: design and demonstration for iron oxide nanoparticle co-precipitation synthesis, Chem. Eng. Sci. 251 (2022), 117481, 10 pp.

[39] B. Chen, Z. Guo, C. Guo, Y. Mao, Z. Qin, D. Ye, F. Zang, Z. Lou, Z. Zhang, M. Li, Y. Liu, M. Ji, J. Sun, N. Gu, Moderate cooling coprecipitation for extremely small iron oxide as a pH dependent T_1-MRI contrast agent, Nanoscale 12 (2020) 5521–5532.

[40] J. Polte, Fundamental growth principles of colloidal metal nanoparticles - a new perspective, CrystEngComm 17 (2015) 6809–6830.

[41] L. Panariello, L. Mazzei, A. Gavriilidis, Modelling the synthesis of nanoparticles in continuous microreactors: the role of diffusion and residence time distribution on nanoparticle characteristics, Chem. Eng. J. 350 (2018) 1144–1154.

[42] H.C. Roth, S.P. Schwaminger, M. Schindler, F.E. Wagner, S. Berensmeier, Influencing factors in the CO-precipitation process of superparamagnetic iron oxide nano particles: a model based study, J. Magn. Magn. Mater. 377 (2015) 81–89.

[43] S. Laurent, D. Forge, M. Port, A. Roch, C. Robic, L. Vander Elst, R.N. Muller, Magnetic iron oxide nanoparticles: synthesis, stabilization, vectorization, physicochemical characterizations and biological applications, Chem. Rev. 108 (2008) 2064–2110.

[44] T. Colla, P.S. Mohanty, S. Nöjd, E. Bialik, A. Riede, P. Schurtenberger, C.N. Likos, Self-assembly of ionic microgels driven by an alternating electric field: theory, simulations, and experiments, ACS Nano 12 (2018) 4321–4337.

[45] Q. Wan, L. Xie, L. Gao, Z. Wang, X. Nan, H. Lei, X. Long, Z.Y. Chen, C.Y. He, G. Liu, X. Liu, B. Qiu, Self-assembled magnetic theranostic nanoparticles for highly sensitive MRI of minicircle DNA delivery, Nanoscale 5 (2013) 744–752.

[46] S. Davidović, V. Lazić, I. Vukoje, J. Papan, S.P. Anhrenkiel, S. Dimitrijević, J. M. Nedeljković, Dextran coated silver nanoparticles — Chemical sensor for selective cysteine detection, Colloids Surf. B Biointerfaces 160 (2017) 184–191.

[47] M. Balas, C.S. Ciobanu, C. Burtea, M.S. Stan, E. Bezirtzoglou, D. Predoi, A. Dinischiotu, Synthesis, characterization, and toxicity evaluation of dextran-coated iron oxide nanoparticles, Metals 7 (2017) 17 (Basel).

[48] A. Bahadur, A. Saeed, M. Shoaib, S. Iqbal, M.I. Bashir, M. Waqas, M.N. Hussain, N. Abbas, Eco-friendly synthesis of magnetite (Fe_3O_4) nanoparticles with tunable size: dielectric, magnetic, thermal and optical studies, Mater. Chem. Phys. 198 (2017) 229–235.

[49] D. Rossi, L. Gargiulo, G. Valitov, A. Gavriilidis, L. Mazzei, Experimental characterization of axial dispersion in coiled flow inverters, Chem. Eng. Res. Des. 120 (2017) 159–170.